

Non-destructive characterization of steel fiber distribution in concrete: CT-scanning vs inductive method

Álvaro Mena-Alonso¹[0000-0002-4269-5299], Guillem Rojas²[0009-0003-1258-3047], Álvaro Muñoz³, Terje Kanstad²[0000-0003-0760-2322] and Miguel A. Vicente¹[0000-0002-9425-6087]

¹ Department of Civil Engineering, University of Burgos (UBU), 09001 Burgos, Spain

² Department of Structural Engineering, Norwegian University of Science and Technology (NTNU), 7034 Trondheim, Norway

³ Stratum Reservoir AS, 4033 Stavanger, Norway

Abstract. This paper presents a robust and comprehensive approach for evaluating the distribution of steel fibers in fiber-reinforced concrete. Two techniques are applied and compared: computed tomography (CT) scanning and inductive testing. Both methods were used on specimens extracted from structural elements, enabling a comparative analysis of fiber distribution and orientation.

The CT and inductive test data were processed to determine the steel fiber content and spatial orientation in each specimen, and the results were then compared. Additionally, the potential of dual-energy computed tomography (DECT) was explored, and several observations regarding its applicability were discussed.

The findings show that both techniques achieve comparable accuracy and consistency in measuring fiber density and orientation. Since CT scanning is regarded as the reference method, the strong agreement between results validates the reliability of the inductive method. Furthermore, the study highlights the potential of DECT as a complementary tool for research in fiber-reinforced concrete.

Keywords: Fiber-reinforced concrete, fiber orientation, computed tomography, inductive method.

1 Introduction

Fiber-reinforced concrete (FRC) is a composite material that, thanks to the load-bearing mechanism provided by fibers bridging across crack surfaces, exhibits high residual strength and toughness after cracking [1]. Over the past decades, scientific interest in FRC has grown significantly, which in turn has increased its use as a partial or even complete replacement for traditional reinforcement bars in reinforced concrete. These technological advances are driving the transition of FRC from its traditional applications in industrial floors, tunnels, etc., to more structurally demanding uses, such as elevated slabs, tunnel segments, and others. However, one of the drawbacks of adding fibers is reduced workability, which is typically mitigated by production techniques

such as glued fibers. In fact, numerous studies have investigated the impact of casting methods and FRC mix design on both workability and mechanical performance [2–4].

The incorporation of fibers improves the tensile behavior of concrete, enabling stress transfer across cracked sections, which increases toughness. This capacity depends on the properties of the matrix, but especially on the amount and orientation of fibers located in the cracked zones. Under certain conditions, strain-hardening behavior can even be achieved [5].

The orientation of fibers has a significant impact on their structural efficiency, ranging from 100% when fibers are perpendicular to the crack plane to about 33% when randomly oriented [6]. However, this effect depends on the fiber type —hooked-end fibers are less sensitive to orientation than straight ones [7]. In any case, controlling fiber orientation during the manufacturing process remains a challenge.

It is commonly assumed that fibers are randomly distributed within concrete. However, scientific literature shows that FRC is an anisotropic material. Properties such as the rheology of the mix, casting method, wall effects, and the presence of obstacles can induce preferential fiber orientations [8]. Consequently, to accurately characterize the mechanical behavior of FRC, it is essential to consider the anisotropy caused by fiber orientation and content [8–10]. Therefore, reliable and cost-effective methods are needed to evaluate the distribution and orientation of fibers in structural elements.

This study compares two methods for determining fiber distribution and orientation: computed tomography (CT) and the inductive method (IM).

CT is a direct method based on the differential attenuation of X-rays as they pass through materials, which depends on density. Scanning a specimen yields a series of grayscale images of its cross-sections. Using appropriate post-processing techniques, it is possible to isolate the different phases within the sample and extract the geometric properties of its components.

This method is particularly effective when there is a significant density difference between the phases. For this reason, it has become the reference technique for analyzing steel fibers in FRC. CT allows for the visualization of the exact position of all fibers and provides individual properties such as volume, location, orientation, and more [9,11].

Additionally, there is a complementary technique known as dual-energy computed tomography (DECT), which combines two X-ray energy spectra to visualize the internal structure of materials. Compared to standard CT, DECT offers the advantage of enabling the determination of absolute densities, making it particularly useful for the analysis of soils and rocks. This study explores the potential of DECT for investigating FRC.

On the other hand, the IM is an indirect method that calculates the content and orientation of steel fibers based on variations in electromagnetic induction [2,12]. One of its limitations is that, at present, the size of IM devices only allows their use on cores and small specimens, but not on larger elements —though this limitation also applies to CT.

This work presents an experimental study that analyzes the distribution of steel fibers in FRC specimens extracted from structural elements. Both CT and IM are used in the analyses, and their performance is compared.

2 Experimental program

2.1 Materials and specimens

The research was carried out on cylindrical cores of steel fiber reinforced concrete (SFRC), extracted from structural elements produced in two experimental programs. Full details of these programs are provided in [13].

Table 1 presents the mix designs of the two types of concrete used: that of Program 1 (B1) and Program 2 (B2). In both cases, the fiber content was 35 kg/m^3 . The fibers used in both programs were of the hooked-end type, with a length of 60 mm and an aspect ratio of 67. The specific models were DE 60/0.9 N from KrampeHarex for Program 1, and 4D 65/60 from Bekaert for Program 2.

The analyzed specimens from Program 1 were labeled P13-4, P13-6, P14-3, and P14-4, and were extracted from slabs with overall dimensions of $1.2 \times 1.2 \times 0.15 \text{ m}^3$. The analyzed specimens from Program 2 were labeled W1-4, W1-12, W1-28, and W4-30, and were extracted from walls with dimensions of $7.0 \times 2.5 \times 0.2 \text{ m}^3$. All specimens underwent inductive method (IM) testing at the NTNU facilities in Trondheim (Norway), and were later analyzed using computed tomography (CT) at Stratum Reservoir AS in Stavanger (Norway). Each specimen was properly identified, clearly indicating its orientation relative to the structural element from which it was extracted.

Table 1. Mix design.

Materials (kg/m^3)	B1	B2
Cement	341	384
Silica fume	22	25
Fly ash	74	17
Water reducing admixture	7.1	2.9
Air entrainer	-	2.0
Water	183	190
Sand, natural 0-8 mm	1012	1100
Stone, crushed 11-16 mm	510	580
Stone, crushed 16-22 mm	170	-
Fibers	35	35

2.2 CT-scanning and postprocessing

The CT scans, as well as the DECT analysis, were carried out at the facilities of Stratum Reservoir AS in Stavanger (Norway). A seventh-generation Toshiba Aquilion Prime helical scanner was used, operating at energy levels with voltages and currents of 135 kV/50 mA and 100 kV/300 mA.

The result of a CT scan is a tomogram—that is, a set of grayscale images representing the cross-sections of the sample, in which darker pixels correspond to less dense

materials and lighter pixels to denser materials. However, the true value of CT lies in the post-processing of the images. In the case of the cores, the goal of post-processing is to segment the fibers; that is, to individually identify all fibers and obtain their morphological properties: center of mass position, length, volume, and orientations.

The procedure followed is summarized in the steps below and illustrated in Figure 1. First, the images are loaded into the image analysis software Dragonfly by ORS. Second, a series of sharpening filters is applied. Third, a segmentation model based on convolutional neural networks (CNNs), specifically developed and calibrated for these specimens, is applied. These models are highly powerful and yield excellent results, especially when there are large quantities of fibers that make separation difficult using conventional segmentation methods. Fourth, once the fibers are segmented, their individual properties are obtained—these correspond to the properties of each volume element identified as a fiber. Finally, the data are exported for statistical analysis.

It is worth mentioning that the following Cartesian coordinate system was used: the Z-axis coincides with the vertical axis of the cylinder, the X-axis is aligned with the hypotenuse of the isosceles right triangle attached to the surface of the specimens, and the Y-axis is aligned with the triangle's axis of symmetry. The Y-axis indicates the concrete casting direction in the structural element.

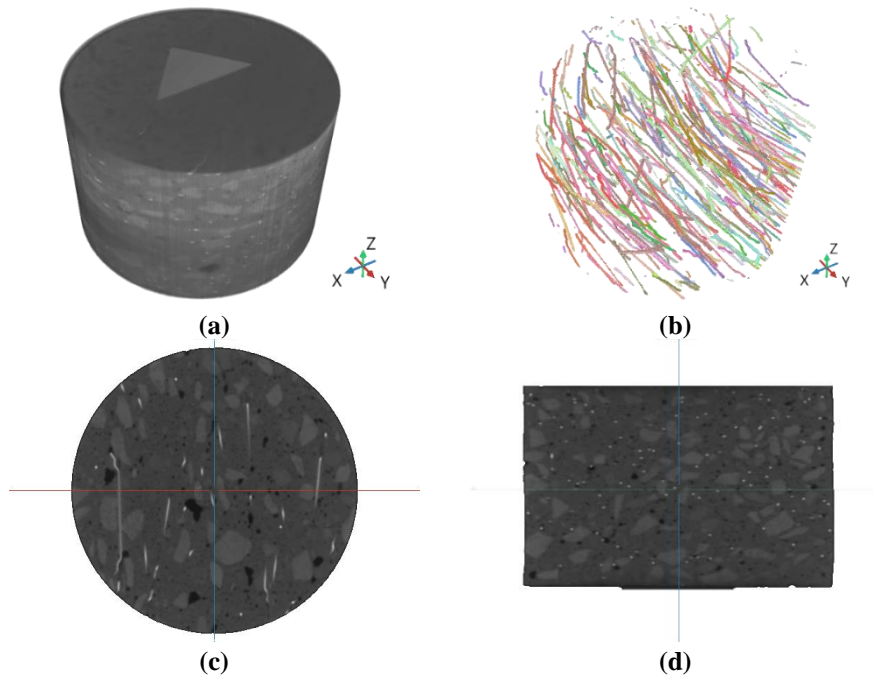


Fig. 1. CT analysis of specimen W1-28: (a) 3D reconstruction, (b) fiber segmentation, (c) cross-section in XY-plane, (d) cross-section in XZ plane.

To characterize fiber orientation, the orientation factor η_θ was used, which is defined as the average projection of the unit vector of the fibers onto a given direction [14]. It is expressed as (Eq.(1)):

$$\eta_\theta = \frac{1}{N_f} \sum_{i=1}^{N_f} \cos \alpha_i^\theta \quad (1)$$

where α_i^θ is the angle between the i -th fiber and the direction of the θ axis, and N_f is the total number of fibers. The values of η_θ range from 0 to 1, where 1 means that all fibers are parallel to the θ axis, and 0 means that all are perpendicular. In this way, three orientation factors can be defined, referred to as η_X , η_Y , and η_Z , corresponding to the X, Y, and Z axes, respectively.

The orientation factors can be visualized in a three-dimensional graph using an ellipsoid, where the eigenvectors a_i and eigenvalues λ_i define the direction and the squared length of the ellipsoid's principal axes, respectively. The ellipsoid can be plotted to represent the dominant fiber direction in the sample. Its spherical shape indicates an isotropic fiber distribution.

If the intersection of the ellipsoid with the XY plane is calculated, an ellipse is obtained. This ellipse represents the dominant direction of the fibers projected onto the XY plane (Figure 2).

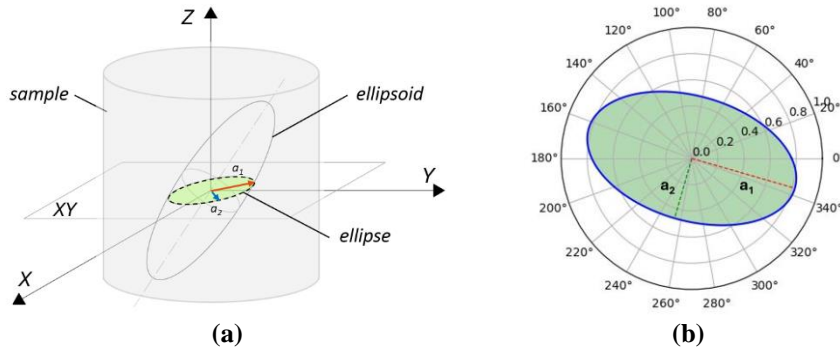


Fig. 2. (a) Ellipsoid and ellipse resulted of the intersection with XY-plane, (b) Representation of the CT orientation ellipse in polar coordinates.

2.3 Inductive method

The inductive test was carried out using the SmartFibreC© equipment by Smart Engineering, which consists of an inductive coil and a digital controller to record the results (Figure 3a). The operation is based on the principle that the total equivalent inductance (L_e) is linearly related to the fiber content (C_f). Through a calibration process—knowing the exact fiber content in several specimens and subsequently crushing them—it is possible to determine the proportionality constant β (Eq. (2)). Recalibration of β is required when the fiber type changes, but not when the concrete mix or specimen shape varies.

$$C_f = \beta \cdot \sum_{x,y,z} \frac{L_i}{B_{V,i}} = \beta \cdot L_e \quad (2)$$

Regarding fiber orientation, the orientation factor is calculated using the following formulation (Eq. (3)), which is specifically adapted for cylindrical specimens. In this expression, ϑ , μ , and $B_{V,i}$ are parameters that depend on the specimen type, γ is a fitting parameter related to the fiber type, and L_e and L_i are inductance measurements along predefined directions.

$$\eta_i = \vartheta \cdot \sqrt{\frac{L_i \cdot (1+2\gamma) \cdot L_e \cdot B_{V,i} \cdot \gamma}{L_e \cdot B_{V,i} \cdot (1-\gamma)}} - \mu \quad (3)$$

The orientation factors in the X and Y directions can be represented in a plane perpendicular to the vertical axis as an ellipse. In Figure 3b, the maximum and minimum orientation factors (η_{\max} and η_{\min}) are shown, corresponding to the major and minor axes of the ellipse. This representation of fiber orientation, equivalent to the one shown in Figure 2 for CT results, has been adopted to compare both methods. It is worth noting that the graphical representation in Figure 3b is a simplified version intended for comparison purposes.

When comparing IM and CT, it becomes evident that IM has several competitive advantages: lower equipment cost, easier operation, compact devices that allow for on-site use, and shorter processing times (CT requires several hours, whereas IM, with prior calibration, takes only about 5 minutes). These features make IM particularly well-suited for applications such as routine quality control. As for its limitations, IM only works with ferromagnetic fibers, and in hybrid concrete, the presence of reinforcement bars affects the results.

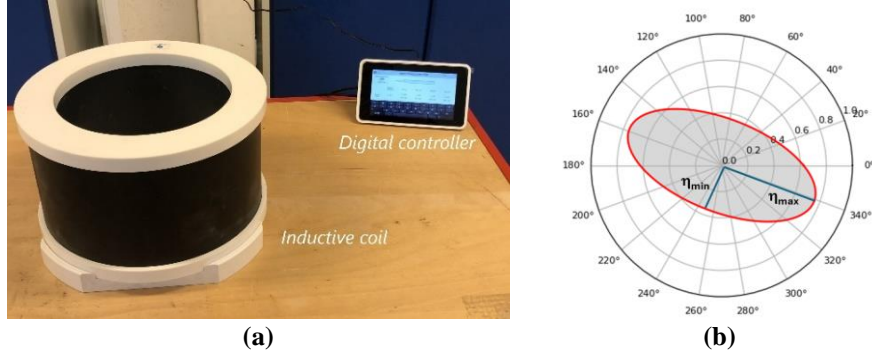


Fig. 3. (a) Inductive method device, (b) Representation of the IM orientation ellipse in polar coordinates.

3 Results

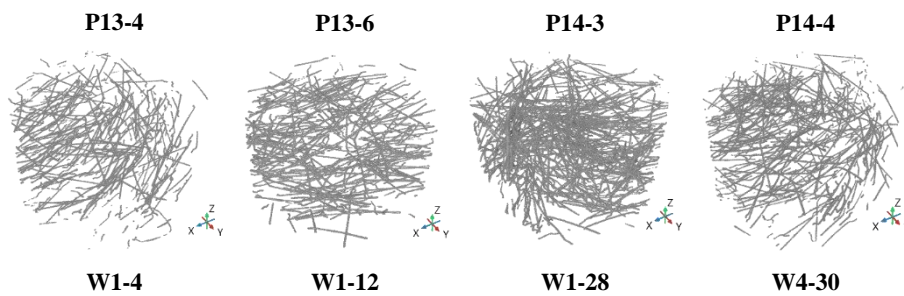
3.1 CT-scanning

Table 2 presents the number of fibers in each specimen, as well as the mean fiber orientation angles per specimen, all obtained from the post-processing of the CT images. It can be observed that in all specimens, the fibers are predominantly aligned within the horizontal XY plane, although the specimens from series B2 show a higher degree of alignment in this plane. Additionally, within the XY plane, the fiber orientation appears to be random, with no clear directional trend, which is expected in cores extracted from surface structural elements.

On the other hand, Figure 4 shows the 3D reconstruction of the fibers in all specimens. These images allow for a visual exploration of the different orientation trends. To aid interpretation, the coordinate system is included.

Table 2. CT results. Number of fibers and average fiber orientation angles with respect to the coordinate axes.

Specimen	N _f	$\alpha_{X,avg}$ [°]	$\alpha_{Y,avg}$ [°]	$\alpha_{Z,avg}$ [°]
P13-4	311	35.6	60.0	78.2
P13-6	327	34.8	62.2	76.5
P14-3	586	51.6	75.3	
P14-4	365	35.1	61.6	77.1
W1-4	251	70.5	22.3	83.5
W1-12	367	51.0	44.4	79.3
W1-28	275	81.7	12.4	82.9
W4-30	307	19.0	75.6	81.4



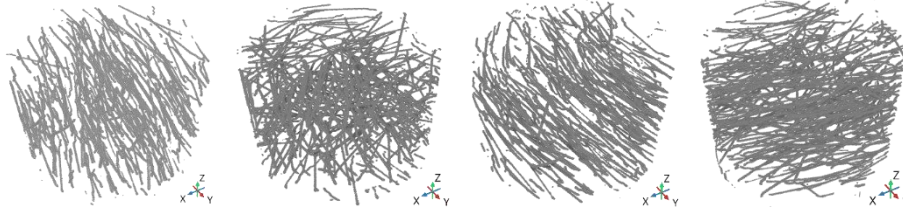
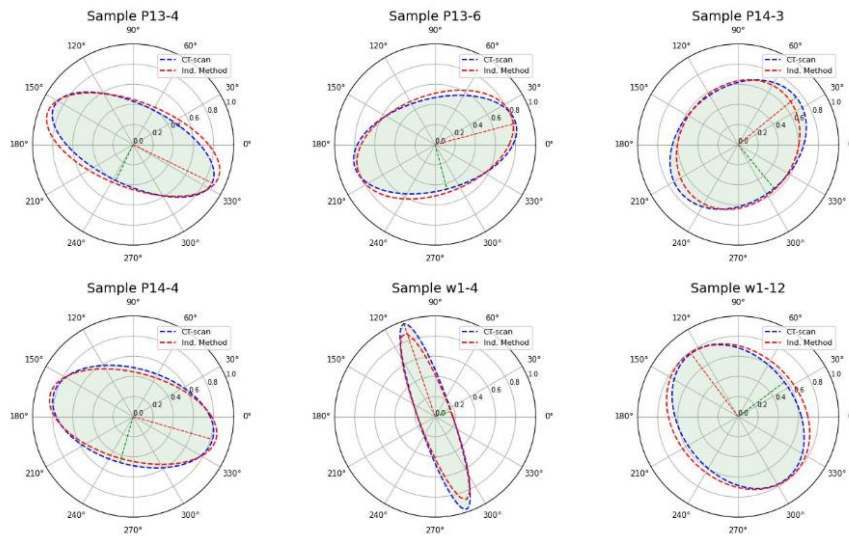


Fig. 4. 3D representation of steel fibers in all specimens.

3.2 Comparison between CT-scanning and inductive method

Figure 5 compares the ellipses representing the dominant fiber orientations in the XY plane, showing the results from CT scanning (in blue) and the inductive method (in red). In both cases, the principal semi-axes of the ellipses correspond to the maximum and minimum values of the orientation factor (η_{\max} and η_{\min}).

Figure 5 confirms the strong correlation between the results of both methods, even when considering samples with a wide variety of fiber orientations. The shape of the ellipses indicates the degree of anisotropy in the fiber distribution: the more elongated the ellipses, the greater the alignment of fibers in a preferred direction. It can be observed that, in all cases, the shapes of the ellipses obtained from both methods are very similar.



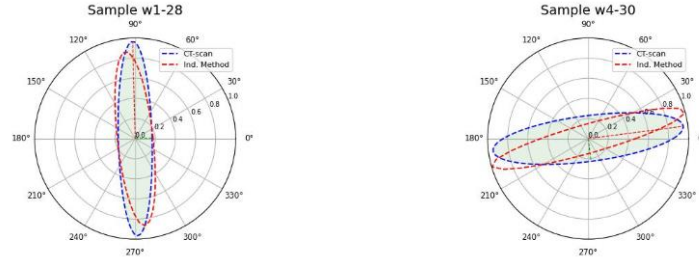


Fig. 5. Comparison between orientation ellipses obtained from CT-scanning (in blue) and the inductive method (in red).

Table 3 presents the results for fiber content in kg/m^3 (C_f) and orientation factors along the three coordinate axes (η_x , η_y , and η_z). The results show a high degree of consistency. It is also observed that the fiber content measured by CT and the inductive method are very similar. The largest discrepancy is found in the Z-direction orientation factor, while good agreement is achieved in the X and Y directions, as also confirmed in Figure 5.

Figure 6 graphically compares the values obtained from CT scanning and the inductive method. In Figure 6a, it can be seen that the C_f values fall within a $\pm 10\%$ deviation range, except for two specimens. Regarding the orientation factors, a good correlation is also observed, with all η_x and η_y values falling within the $\pm 15\%$ range. The η_z values show lower correlation, as the inductive method tends to yield higher values compared to those obtained with CT scanning. This observation highlights the need for a more in-depth study of this phenomenon, using a larger number of samples. In any case, the correlation is acceptable.

Table 3. CT results. Number of fibers and average fiber orientation angles with respect to the coordinate axes.

Specimen	CT-scanning				Inductive method			
	C_f [kg/m ³]	η_x	η_y	η_z	C_f [kg/m ³]	η_x	η_y	η_z
P13-4	29.6	0.78	0.46	0.21	28.0	0.72	0.43	0.31
P13-6	33.7	0.78	0.41	0.23	31.4	0.65	0.45	0.40
P14-3	63.5	0.64	0.59	0.27	58.9	0.51	0.54	0.48
P14-4	36.7	0.76	0.42	0.23	35.9	0.69	0.39	0.39
W1-4	25.4	0.32	0.92	0.10	23.3	0.33	0.82	0.17
W1-12	38.2	0.59	0.65	0.17	33.3	0.59	0.60	0.27
W1-28	27.5	0.13	0.97	0.11	28.3	0.20	0.87	0.19
W4-30	31.9	0.94	0.21	0.14	36.4	0.82	0.16	0.34

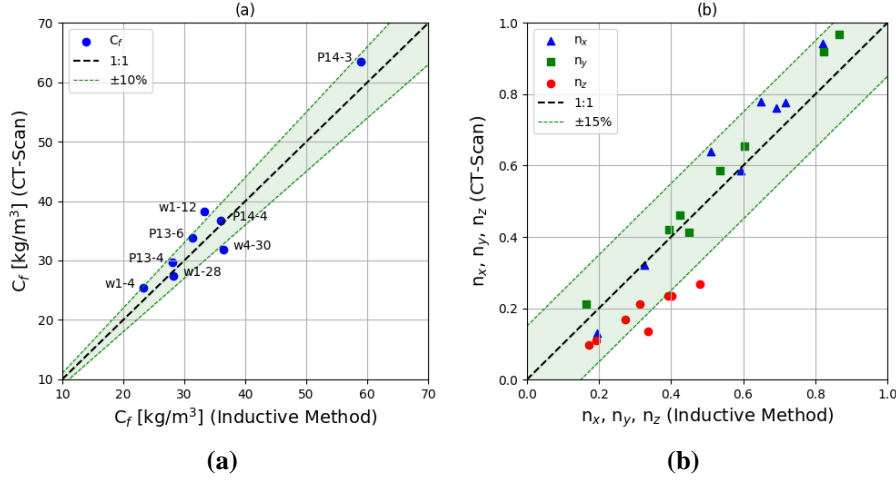


Fig. 6. Correlation between the results of CT-scanning and the inductive method: (a) fiber content, (b) fiber orientation factors.

3.3 Additional results provided by DECT

Table 4 summarizes the results obtained from dual-energy computed tomography in terms of apparent density (ρ_b) in kg/m^3 , effective atomic number (Z_{eff}), photoelectric factor (P_e), and apparent porosity (ϕ_{ap}).

Table 4. DECT results. Values of the main parameters.

Specimen	ρ_b [T/m^3]	Z_{eff}	P_e	ϕ_{ap} (%)
P13-4	2.32	6.95	1.18	10.6
P13-6	2.40	7.11	0.91	7.6
P14-3	2.43	4.40	0.43	6.7
P14-4	2.33	7.43	1.56	10.9
W1-4	2.30	13.17	3.62	11.7
W1-12	2.45	12.54	3.03	6.0
W1-28	2.40	12.27	3.01	7.7
W4-30	2.43	12.47	3.11	6.6

Several interesting conclusions can be drawn from Table 4. First, despite a difference of more than 38 kg/m^3 between the sample with the lowest fiber content (W1-4) and the one with the highest volume (P14-3), the data show only a 5-6% reduction in porosity. This indicates that although the fibers occupy additional volume, they are not able to block the pore space due to their irregular distribution. No clear relationship is observed between apparent porosity and fiber content as determined by the applied

method, since an increase in fiber content does not necessarily result in a significant reduction in porosity.

Second, regarding apparent density, a correlation has been observed between the amount of steel fibers and the measured ρ_b , with a low value of 2.29 T/m³ for W1-4, while values increase to 2.43 and 2.45 T/m³ in samples P14-3 and W1-12, respectively (Table 4). However, due to the low design fiber content in the specimens (0.45%), this effect is relatively minor, and the total increase in density cannot be explained solely by the increase in fiber content.

4 Conclusions

This study presents a reliable and comprehensive comparison between CT-scanning and the inductive method for evaluating the distribution and orientation of steel fibers in fiber-reinforced concrete. The specimens analyzed were cores extracted directly from large structural elements.

The results confirm that CT scanning, combined with appropriate post-processing software, allows for the accurate reconstruction of 3D fiber distributions in the concrete matrix without damaging the sample. This enables the quantification of both fiber content and dominant orientation.

The inductive method also proved capable of predicting fiber content and orientation, including the directions corresponding to maximum and minimum orientation values in cylindrical specimens. The results from both techniques showed a high level of agreement in terms of fiber density and spatial orientation, validating the inductive method when CT is considered the reference.

Although CT scanning provides more detailed information—including data on porosity, cracks, and aggregate distribution—the inductive method offers clear advantages in terms of speed, cost, and ease of use. Its main limitation is that it only applies to ferromagnetic fibers.

Both techniques are suitable for quality control. While the sample volume is small compared to the entire structural element, the insights gained on fiber distribution and orientation are highly valuable.

Finally, DECT was used to provide complementary data. While it supported many of the conclusions, some parameters inconsistent correlations, likely due to the use of a central line probe. Future research should consider full-volume DECT analysis to better understand the relationship between these parameters and fiber distribution.

References

1. Barros, J.A., et al., *Post-cracking behaviour of steel fibre reinforced concrete*. Materials and Structures, 2005. 38: p. 47-56.
2. Torrents, J.M., et al., *Inductive method for assessing the amount and orientation of steel fibers in concrete*. Materials and structures, 2012. 45: p. 1577-1592.

3. Zhou, B. and Y. Uchida, *Influence of flowability, casting time and formwork geometry on fiber orientation and mechanical properties of UHPFRC*. Cement and Concrete Research, 2017. 95: p. 164-177.
4. Žirgulis, G., et al., *Importance of quantification of steel fibre orientation for residual flexural tensile strength in FRC*. Materials and structures, 2015. 49(9): p. 3861-3877.
5. Gesoglu, M., et al., *Strain hardening ultra-high performance fiber reinforced cementitious composites: Effect of fiber type and concentration*. Composites Part B: Engineering, 2016. 103: p. 74-83.
6. Thorenfeldt, E., *Theoretical tensile strength after cracking. Fibre orientation and average stress in fibres*. Nordic Miniseminar Oslo, Norway. The Norwegian Concrete Association. Proceedings of the Nordic Concrete Federation Workshop on Design Rules for Steel Fibre Reinforced Concrete Structures, 2003: p. 43-60.
7. Gebuhr, G., et al., *Analysis and evaluation of the pull-out behavior of hooked steel fibers embedded in high and ultra-high performance concrete for calibration of numerical models*. Structural Concrete, 2019. 20(4): p. 1254-1264.
8. Alberti, M., A. Enfedaque, and J. Gálvez, *A review on the assessment and prediction of the orientation and distribution of fibres for concrete*. Composites Part B: Engineering, 2018. 151: p. 274-290.
9. Vicente, M.A., et al., *Effects of fiber orientation and content on the static and fatigue behavior of SFRC by using CT-Scan technology*. International Journal of Fatigue, 2019. 128: p. 105178.
10. Skarżyński, Ł. and J. Suchorzewski, *Mechanical and fracture properties of concrete reinforced with recycled and industrial steel fibers using Digital Image Correlation technique and X-ray micro computed tomography*. Construction and Building Materials, 2018. 183: p. 283-299.
11. Mena-Alonso, Á., et al., *La tomografía computerizada más allá de la medicina: Aplicaciones al estudio microestructural del hormigón y otros materiales de la ingeniería*. Hormigón y acero, 2020. 71(292): p. 7-19.
12. Cavalaro, S.H.P., et al., *Improved assessment of fibre content and orientation with inductive method in SFRC*. Materials and Structures, 2015. 48: p. 1859-1873.
13. Rojas, G. and T. Kanstad, *Testing and modelling of horizontally and vertically cast FRC elements*, in XI International Symposium on Fiber Reinforced Concrete (BEFIB 2024), Dresden, Germany. 2024.
14. Lorente, S., S. Carmona, and C. Molins, *Use of fiber orientation factor to determine residual strength of steel fiber reinforced concrete*. Construction and Building Materials, 2022. 360: p. 128878.